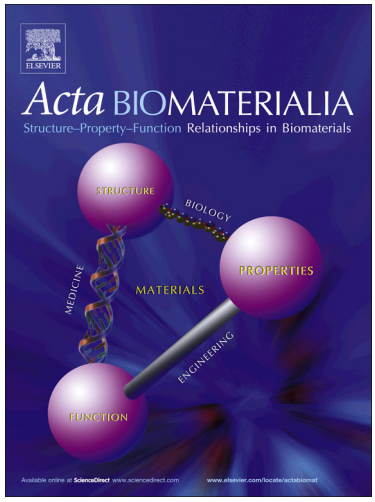

Design, Development and Characterization of Synthetic Bruch's Membranes

Denver C. Surrao, Ursula Greferath, Yu-Qian Chau, Stuart J. Skabo, Mario Huynh, Kinnari J. Shelat, Ioannis J. Limnios, Erica L. Fletcher, Qin Liu

PII: S1742-7061(17)30604-9
DOI: https://doi.org/10.1016/j.actbio.2017.09.032
Reference: ACTBIO 5094

To appear in: *Acta Biomaterialia*

Received Date: 12 April 2017
Revised Date: 13 September 2017
Accepted Date: 22 September 2017

Please cite this article as: Surrao, D.C., Greferath, U., Chau, Y-Q., Skabo, S.J., Huynh, M., Shelat, K.J., Limnios, I.J., Fletcher, E.L., Liu, Q., Design, Development and Characterization of Synthetic Bruch's Membranes, *Acta Biomaterialia* (2017), doi: https://doi.org/10.1016/j.actbio.2017.09.032

Design, Development and Characterization of Synthetic Bruch's Membranes

Denver C. Surrao[1*], Ursula Greferath[2], Yu-Qian Chau[1], Stuart J. Skabo[1], Mario Huynh[2], Kinnari J. Shelat[3,4], Ioannis J. Limnios[1], Erica L. Fletcher[2] and Qin Liu[1]

[1] Clem Jones Research Centre for Regenerative Medicine, Faculty of Health Sciences and Medicine, Bond University, Gold Coast, QLD 4229, Australia

[2] Department of Anatomy and Neuroscience, The University of Melbourne, Melbourne, VIC 3010, Australia

[3] Australian Institute for Bioengineering and Nanotechnology (AIBN), The University of Queensland, Brisbane, QLD 4072, Australia

[4] Australian National Fabrication Facility (ANFF), Queensland Node, The University of Queensland, Brisbane, QLD 4072, Australia

[*] **Corresponding Author**

Dr. Denver C. Surrao
Clem Jones Research Centre for Regenerative Medicine
Faculty of Health Sciences and Medicine
Bond University
Gold Coast, QLD 4229
Australia

Phone: +61 7 5595 4195
Fax: +61 7 5595 4538
Email: dsurrao@bond.edu.au

Abstract

Age-related macular degeneration (AMD) is a leading cause of blindness, and dry AMD has no effective treatment. Retinal constructs comprising retinal pigment epithelium (RPE) cells supported by electrospun scaffolds have been investigated to treat dry AMD. However, electrospun scaffolds studied to-date do not mimic the structural microenvironment of human Bruch's membrane (BM), essential for native-like RPE monolayers. The aim of this study was to develop a structurally biomimetic scaffold designed to support a functional RPE monolayer, comprising porous, electrospun nanofibrous membranes (ENMs), coated with laminin, mimicking the inner collagenous layer (ICL) and basal RPE lamina respectively, the cell supporting layers of the BM. *In vitro* evaluation showed 70 nm PLLA ENMs adsorbed high amounts of laminin and supported functional RPE monolayers, exhibiting 3D polygonal-cobblestone morphology, apical microvilli, basal infoldings, high transepithelial resistance (TER), phagocytic activity and expression of signature RPE markers. 70 nm PLLA ENMs were successfully implanted into the subretinal space of RCS-rdy+p+/LAV rats, also commonly know as *rdy* rats. At week 4, in the absence of immunosuppressants, implanted PLLA ENMs were surrounded by a significantly low number of activated microglial cells, compared to week 1, indicating no adverse long-term immune response. In conclusion, we successfully designed and tested ENMs emulating the RPE cell supporting layers of the BM, and found 70 nm PLLA ENMs to be best suited as scaffolds for fabricating retinal constructs.

Keywords: age-related macular degeneration (AMD), Bruch's membrane (BM), 70 nm electrospun nanofibrous membranes (ENMs), human retinal pigment epithelium (hRPE) cells, RPE functionality, subretinal implantation

1. Introduction

Age related macular degeneration (AMD) is a leading cause of vision loss in the developed world [1-3], with more than 14 million people suffering from blindness or severe visual impairment [1-3]. The two subtypes of AMD include: dry (non-neovascular), and wet (neovascular) AMD [2-4]. Dry AMD accounts for a majority of cases and has no effective treatment [1,4]. While wet AMD is progressive and partially controlled via intravitreal anti-VEGF injections [1,4]. The initial pathologic damage in dry AMD results from age-accumulated dysfunction of the Bruch's membrane (BM) and retinal pigment epithelium (RPE) cells [1,5].

Native human BM is a 5 μm thick, semi-permeable membrane, composed of five layers, including a basal RPE lamina membrane, an inner collagenous layer (ICL), an elastin layer (EL), an outer collagenous layer (OCL), and a basement membrane of the choriocapillaris [6,7]. The semi-permeable nature of the BM helps regulate the diffusion of biomolecules, nutrients, oxygen, fluids and metabolic waste between the retina and the underlying choroid [3,6,7]. The BM also provides physical support for the adhesion, and formation of a functional RPE monolayer, and acts as a barrier, inhibiting cell migration between the choroid and retina [3,6,7]. RPE cells have distinct apical microvilli and basal infoldings, and are responsible for absorption of stray light, maintenance of the visual cycle, phagocytosis of shed photoreceptor outer segments (POS) and secretion of various cytokines to maintain retinal function [3,8,9]. The RPE monolayer and BM together are essential for maintaining the health and function of photoreceptors, which send visual signals to the optic nerve and brain [3,8,9]. Damage to RPE cells and BM leads to photoreceptor dysfunction, leading to vision reduction, and eventually photoreceptor death and vision loss [3,8]. Therapies that replace diseased RPE cells with functional cells are promising [8,9]. In AMD patients, however, age-related changes to the ICL negatively impacts attachment and survival of injected RPE cells [5,6,8], causing them to clump, triggering retinal fibrosis [3,8].

Researchers have re-engineered young human BMs to support RPE cells by refurbishing with laminin, vitronectin or fibronectin after appropriate tissue processing [10-12]. Limited donor tissue and disease transmission, however, makes refurbished BMs an impractical solution to treat dry AMD [8]. Studies have shown the basal RPE lamina and ICL layers to be critical for RPE cell proliferation and function, with support for RPE cells decreasing, further the layer is from the basal RPE lamina membrane [11,12]. It is therefore critical to design and develop biomimetic scaffolds that can replace diseased BMs, capable of supporting a functional RPE monolayer. Such a biomimetic scaffold needs to be biocompatible, possess mechanical properties that aids in subretinal implantation, and mirror the microenvironment of RPE cell supporting layers [3]. Various groups have used synthetic, polymer based electrospun membranes as scaffolds to support RPE monolayers [13-17]. These scaffolds have a wide range of physical properties, but do not mimic the microenvironment of the RPE cell supporting layers, required for development of a functional RPE monolayer [1,6,18,19]. The best published synthetic membrane possess an average fibre diameter of 130 nm [13] which is two-fold larger than the average fibre diameter (70 nm [6,7]) of the collagen fibres that constitute the ICL.

Our aim was to design, develop and evaluate synthetic biomimetic-like scaffolds, comprising porous, electrospun nanofibrous membranes (ENMs), coated with laminin best suited for retinal tissue engineering. The

laminin coating will mimic the basal RPE lamina membrane, a 0.15 μm thick meshwork of fine fibers [6,7], facilitating RPE cell adhesion [3,8,20]. While porous ENMs will mimic the ICL, a 1.4 μm thick semi-permeable collagen membrane [6,7], supporting the diffusion of nutrients and oxygen to, and metabolic waste from the overlaying RPE monolayer [3,8]. We also tested the biocompatibility of the best ENM, evaluated via *in vivo* studies, by implanting it into the subretinal space of RCS-rdy+p+/LAV rats, a functional-RPE strain commonly known as *rdy* rats. The polymers used to fabricate the ICL included poly(ε-caprolactone) (PCL), poly(L-lactide-*co*-glycolide) (PLGA), poly(L-lactide-*co*-D,L-lactide) (PLDLA) and poly(L-lactide) (PLLA), which are biocompatible and biodegradable [21]. These polymers possess varying hydrophobic properties, which will affect the adsorption [22-24] and conformation [25,26] of laminin on their surfaces. The mechanical properties of these polymers have been shown to influence cell fate [27-29]. We hypothesize that the combined effects of laminin adsorption and optimal mechanical properties, coupled with the creation of a synthetic, porous ICL-like nano-structure could positively influence RPE cells creating a functional monolayer.

2. Materials and methods

2.1 Characterization of polymers

PCL was purchased from Sigma Aldrich, USA. PLLA, PLGA (85:15 L-lactide:glycolide) and PLDLA (70:30 L-lactide:D,L-lactide) were purchased from Corbion, the Netherlands. Number average molecular weight (M_n) and polydispersity index (PDI) were measured using a Viscotek 270max Separation Module, equipped with a refractive index (RI) detector. Two PolyAnalytik columns with an exclusion limit of $20 \cdot 10^6$ g·mol^{-1} were used in series. The calibration curve based on the RI detector was constructed using a polystyrene standard (7 - 844 kDa). Tetrahydrofuran (THF) at 40 °C was used as the mobile phase, and results were analyzed using Astra v4.90.07 software (Wyatt Technology, USA). Mettler Toledo DSC1 System was used to measure thermal properties, including glass transition temperature (T_g), melting point (T_m) and heat of fusion (ΔH_f). Here, polymers were taken through two heating cycles (-80 °C - 200 °C) and one cooling cycle (200 °C to -80 °C), at a 10 °C min^{-1} heating rate with a 3 min hold time at each end point. T_g was determined from the second heating cycle, while T_m and ΔH_f were determined from the first heating cycle. The minimum of the endotherm curve in the first heating cycle was taken as T_m, while area bound by the endotherm normalized to the mass of the polymer sample was used to calculate ΔH_f. Polymer crystallinity (X_c) was calculated by dividing the measured ΔH_f value by ΔH^o for purely crystalline PLLA (93.1 J·g^{-1} [30]), and purely crystalline PCL (139.5 J·g^{-1} [31]).

2.2 Fabrication of electrospun nanofibrous membranes (ENMs)

PCL, PLGA, PLDLA and PLLA were dissolved in a solution of 1,1,1,3,3,3-hexafluoro-2-isopropanol (HFIP, Sigma Aldrich, USA) and phosphate buffer solution (1x PBS, Invitrogen, USA) as listed in Table 1. The electrospinning apparatus consisted of a syringe pump (New Era Pump Systems Inc., USA), high voltage generator (Gamma Voltage Research, USA) and a rotating mandrel. The mandrel was connected to an electric motor and rotated at 100 rpm (linear velocity: 0.42 m·s^{-1}). Polymer solutions were pumped at a flow rate of 1

$mL \cdot min^{-1}$ through a 23 G blunt tip needle (Livingstone International, Australia). The air gap between the needle and mandrel was 15 cm and a voltage of 1 $kV \cdot cm^{-1}$ was applied. Electrospun membranes were collected on the mandrel and stored in a vacuum desiccator until required.

2.3 Physiochemical characterization of ENMs

2.3.1 Assessment of average fibre diameter, membrane thickness and porosity of ENMs

Flat and cross-sections samples of ENMs were mounted on stubs, gold sputter coated (JEOL Smart Coater, USA) and imaged using a JCM-5000 NeoScope Benchtop SEM (Jeol, USA) equipped with JCM-5000 NeoScope software. From SEM images of flat samples 100 fibres (n = 100) per ENM were analyzed to determine average fibre diameter, and 50 measurements (n = 50) per ENM were analyzed for porosity. Similarly, 50 cross-sectional measurements (n = 50) per ENM were analyzed to determine average membrane thickness.

2.3.2 Assessment of wettability of ENMs

Wettability of ENMs were evaluated using the sessile drop method, where 20 µL of deionized water (Merck Millipore, USA) was dropped onto the ENMs and allowed to stabilize for 10 seconds. The shape of the water droplets on each of the ENMs was recorded and the angle between the tangent of the water droplet and surface of the ENM was measured using an optical contact angle meter (OCA20, Dataphysics Instruments GmbH, Germany). Contact angles were measured at ten different locations (n = 10) for each ENM.

2.3.3 Assessment of topography, surface roughness, surface stiffness and modulus of ENMs

2D and 3D images, surface roughness and mechanical properties of ENMs were measured using a MFP-3D Infinity Atomic force microscope (AFM, Asylum Research, USA). 2D and 3D images were captured in tapping mode, in air using an ETALON cantilever (resonant frequency: 145 Hz and spring constant: 3.5 $N \cdot m^{-1}$). Topography images of ENMs (n = 6) were processed using Asylum Research Analysis (Asylum Research, USA) to determine surface roughness. Mechanical properties of ENMs were determined in contact mode in an aqueous environment using a SiNi cantilever (spring constant: 0.27 $N \cdot m^{-1}$). Moduli of ENMs were calculated by fitting force curves using the Oliver-Pharr model (rate: 1 $\mu m \cdot s^{-1}$ and load: 5 nN). Approximately, 100 force curves at six different locations (n = 6) on the surface of each ENM were used to determine mechanical properties.

2.3.4 Assessment of laminin adsorption on the surface of ENMs

Controls (tissue culture treated coverslips, Nunc™ Thermanox™ Coverslips, 15 mm, Thermo Scientific, USA) and ENMs were coated with 300 µL of mouse laminin (20 $\mu g \cdot mL^{-1}$, Cat# 23017-015, Gibco, USA), incubated for 4 h at 37 °C and 5% CO_2, and then fixed in 4% paraformaldehyde (PFA, Sigma Aldrich, USA) for 15 min. Samples were incubated with primary laminin antibody (1:100, Cat# ab11575, Abcam, USA), reconstituted in cold 3% bovine serum albumin (BSA, Sigma Aldrich, USA). Samples were incubated for 1 h at room temperature (RT) with Alexa Fluor® 488 conjugated secondary antibody (1:400, Invitrogen, USA), and

imaged using a confocal microscope (Nikon C1, Nikon Instruments Inc., USA). Laminin adsorption was also assessed using a micro-BCA™ protein assay kit (Thermo Scientific, USA). Controls and ENMs coated with 20 $\mu g \cdot mL^{-1}$ laminin were incubated for 4 h at 37 °C and 5% CO_2, and washed thrice with 1x PBS. 500 µL of sodium dodecyl sulfate (SDS, 10 $mg \cdot mL^{-1}$, Sigma Aldrich, USA) was added, and samples sonicated for 20 min. Concentration of laminin in SDS solutions were measured using absorbance at 560 nm against a standard laminin curve using a plate reader (Turner Biosystems, USA). Laminin adsorption was determined from six independent samples (n = 6) in triplicate (technical replicates) for each ENM and control.

2.4 *In vitro* studies

2.4.1 Culturing and seeding of human retinal pigment epithelium (hRPE) cells

Clonetics™ human RPE cells (hRPE cells, passage 3, Lonza, USA) were grown in T-75 flasks (Thermo Scientific, USA) coated with 20 $\mu g \cdot mL^{-1}$ of laminin for three population doublings. Controls and ENMs affixed to CellCrown™24 (Scaffdex, Finland) were sterilized via gamma irradiation (25 kGy, Steritech, Australia), coated with 300 µL of laminin (20 $\mu g \cdot mL^{-1}$, Gibco, USA) and incubated for 4 h at 37 °C and 5% CO_2. Supported by literature [2,15-17], hRPE cells were seeded at 10,000 $cells \cdot cm^{-2}$ onto sterilized controls and ENMs, and cultured in Retinal Pigment Epithelial Cell Growth Media (RtEGM™, Lonza, USA) supplemented with RtEGM™ SingleQuots® (Lonza, USA), containing 2% L-glutamine, 2% fetal bovine serum, 0.5% basic fibroblast growth factor, and 0.1% gentamicin sulphate and amphotericin-b (Lonza, USA). The RtEGM™ supplemented culture medium was changed every second day.

2.4.2 Scanning electron microscope (SEM) assessment of hRPE cells on ENMs

Prior to SEM imaging, hRPE cells cultured in laminin coated 24-well plates (controls, Thermo Scientific, USA) and ENMs were fixed in cold 3% glutaraldehyde (Sigma Aldrich, USA). Samples were dehydrated using graded (30%, 50%, 70%, 80%, 90%, 95% and 100%) ethanol solutions, chemically dried using hexamethyldisilazane (HMDS, Sigma Aldrich, USA), and finally air-dried. Dry samples were mounted on stainless steel stubs, gold sputter coated, and imaged using a SEM as described in Section 2.3.1.

2.4.3 Assessment of hRPE cell proliferation and cytotoxicity of ENMs

hRPE cell proliferation and cytotoxicity of ENMs were assessed using WST-1 cell proliferation reagent (Roche Diagnostics, Switzerland), performed 4 h after cell seeding, and on days 1, 3, 7 and 14. On the test day, media was replaced with 900 µL of fresh RtEGM™ supplemented culture media and 100 µL of WST-1 reagent, and incubated at 37 °C and 5% CO_2 for 4 h. 100 µL of media from each test group was transferred to a 96-well plate and absorbance was measured at 450 nm using a plate reader (Turner Biosystems, USA). Cell proliferation and cytotoxicity were determined from six independent samples (n = 6) for each ENM and control (laminin coated 24-well tissue culture plates) in triplicate (technical replicate).

2.4.4 Assessment of transepithelial electrical resistance (TER) of hRPE monolayers on ENMs

TER ($\Omega \cdot cm^2$) of hRPE monolayers cultured on ENMs were determined using a STX2 electrode (World Precision Instruments, USA) connected to an epithelial volt/ohm meter (World Precision Instruments, USA). TER was determined from six independent samples (n = 6) in triplicate (technical replicate) for each ENM, and corrected for background resistance, obtained from cell-free ENMs in RtEGM™ supplemented culture medium.

2.4.5 Assessment of gene expression of hRPE monolayers on ENMs

Total RNA from hRPE monolayers cultured on ENMs and controls (24-well tissue culture plates) were extracted using PureZOL™ RNA (BioRad, USA). RNA concentration and A260:A280 ratio were quantified using a NanoDrop 2000c (Thermo Scientific, USA). One microgram of RNA was reverse transcribed using iScript™ cDNA (BioRad, USA) and quantitative PCR (qPCR) analysis was carried out with SsoFast™ EvaGreen® Supermix (BioRad, USA) on a Corbett Rotor-Gene 6000 RT-PCR thermocycler (Qiagen, USA). qPCR data was determined from four independent samples (n = 4) in triplicate (technical replicate) for each ENM and control. Gene expression data were normalized to GAPDH (Gene ID: 2597), and presented as fold-change relative to week 2 controls. The oligo sequences used in this study are listed in Table 2.

2.4.6 Immunohistochemical (IHC) assessment of hRPE monolayers on ENMs

hRPE monolayers cultured on controls (laminin coated tissue culture treated coverslips), and ENMs were fixed in 4% PFA for 15 min at RT, permeabilized with 0.1% TritonX-100 (Sigma Aldrich, USA) for 15 min, and blocked in cold 3% BSA. Samples were incubated with primary antibodies Cytokeratin 18 (1:100, Cat# ab82254, Abcam, USA), Ki67 (1:400, Cat# ab15580, Abcam, USA), ZO1 (1:100, Cat# 617-300, Invitrogen, USA), MITF (1:500, Cat# ab12039, Abcam, USA), MCT1 (1:50, Cat# ab90582, Abcam, USA) and MerTK (1:25, Cat# PA5-15028, Invitrogen, USA), reconstituted in cold 3% BSA. Samples were washed with 1x PBS and incubated for 1 h at RT in the dark with appropriate Alexa Fluor® conjugated secondary antibodies (1:200, Alexa Fluor® 488, and Alexa Fluor® 568, Invitrogen, USA), counter-stained with DAPI (1:500, Cat# D1306, Invitrogen, USA), and imaged using a Nikon C1 confocal microscope.

2.4.7 Phagocytosis assay for hRPE cells on ENMs

At week 8, hRPE monolayers cultured on controls (24-well, laminin coated tissue culture plates) and ENMs were incubated with 1 mL of RtEGM™ supplemented culture medium, containing Cy3-conjugated polystyrene beads ($1 \cdot 10^8$ beads$\cdot mL^{-1}$, diameter 1 μm, Invitrogen, USA) for 6 h. Samples were washed multiple times with 1x PBS, treated with 1x trypsin (Gibco, USA), and re-seeded as single cells on laminin coated tissue culture treated coverslips to exclude false positive staining caused by externally bound beads. Re-seeded cells were cultured overnight, and fixed with 4% PFA for 15 min at RT, permeabilized with 0.1% TritonX-100 for 15 min and blocked in cold 3% BSA. Samples were incubated overnight at 4 ºC with MerTK (1:25), following which they were washed with 1x PBS and incubated for 1 h at RT in the dark with Alexa Fluor® 568 conjugated

secondary antibody (1:100). Samples were also stained for F-actin using Alexa Fluor® 488 conjugated Phalloidin (1:50, Cat# A12379, Invitrogen, USA) and DAPI (1:500) for 1 h in the dark at RT, and imaged using a Nikon C1 confocal microscope. Number of ingested beads per cell was determined from one hundred (n = 100) independent cell measurements for each ENM and control. A cut-off of ten beads per cell was used to determine percentage-phagocytizing cells for each condition.

2.4.8 Transmission electron microscope (TEM) assessment of hRPE monolayers on PLLA ENMs

hRPE monolayers cultured on PLLA ENMs were washed with 1x PBS, fixed in cold 3% glutaraldehyde, and further postfixed in 1% osmium tetroxide (Sigma Aldrich, USA). Samples were dehydrated through a series of graded (30%, 50%, 70%, 80%, 90%, 95% and 100%) ethanol solutions, infiltrated with resin using a Pelco Biowave (Ted Pella Inc., USA), and polymerized overnight at 60 °C. 80 nm sections were cut using a Leica UC6 ultramicrotome (Leica Microsystems Pty Ltd, Australia), contrasted with uranyl acetate and lead citrate, and imaged using a Joel 1011 Transmission Electron Microscope (TEM, Joel, USA) at 80 kV. TEM images were captured using a Morada G2 digital camera (Olympus, USA).

2.5 *In vivo* studies

2.5.1 Subretinal implantation of PLLA ENMs

Subretinal surgeries in *rdy* rats (congenic, non-dystrophic, controls for Royal College of Surgeons rats) were done in accordance with the University of Melbourne Animal Experimentation Ethics Committee (Ethics # 1312958.4), and the Association for Research in Vision and Ophthalmology (ARVO) statement. 10 µm thick PLLA ENMs were encapsulated in 20 µL gelatin (20 w/v%, Sigma Aldrich, USA), cooled at 4 °C for 5 min, and cut into 0.8 mm discs. *Rdy* rats were anesthetized with a mixture of ketamine (60 mg/kg, Provet, Australia) and xylazine (5 mg/kg, Provet, Australia). Ocular surfaces were administered Alcaine (0.5%, Alcon Laboratories, Australia), and under microscopic observation eyes were rotated to expose the sclera, and insertions made with a 33 G needle. Insertions were widened, and with a 33 G needle gelatin encased ENMs were surgically implanted into the subretinal space of *rdy* rats. In most cases ENMs were bilaterally implanted with a single ENM per eye. The rats were monitored for 5 days post-surgery, and then divided into two groups (week 1 and week 4) with n = 10 per group. A separate cohort of *rdy* rats (n = 6), where the subretinal surgery alone was performed served as age-matched sham operated controls. The *rdy* rats were not administered immunosuppressants.

2.5.2 *In vivo* retinal imaging of implanted PLLA ENMs

At week 1, post-implantation the position of PLLA ENMs in the subretinal space of *rdy* rats were determined using Ocular Coherence Tomography (OCT) and fundus imaging. Rats were anaesthetized, and their eyes were kept lubricated throughout imaging (0.3% Genteal, Alcon Laboratories, Australia). OCT and fundus images were taken using a Micron III rodent fundus camera (Phoenix Research Labs, USA) using specialty Micron III (Phoenix Research Labs, USA) and Streampix (Norpix Inc., Canada) software, respectively.

2.5.3 Histology and IHC assessment of laminin coated PLLA ENMs

Anaesthetized *rdy* rats implanted with laminin coated PLLA ENMs, and sham operated controls were sacrificed with an intracardial injection (100 µL, Lethabarb, Virbac Pty Ltd., Australia). Eyes for paraffin sectioning were fixed overnight in an ethanol solution, containing 4% PFA, 5% acetic acid and 3% sucrose, and dehydrated through a series of graded (70%, 95% and 100%) ethanol solutions. Eyes were then cleared in xylene and embedded in paraffin. 5 µm thick paraffin sections were cut, dewaxed and rehydrated in ethanol (100%, 90% and 70%), and stained with hematoxylin and eosin (H&E). IHC samples were fixed in 4% PFA for 30 min at RT and cryoprotected in a series (10% and 20%) of sucrose solutions, and incubated in cold 30% sucrose overnight. Cryoprotected samples were embedded in Tissue-Tek OCT (Sakura Seiki, Japan) and frozen in cold isopentane (Fisher Scientific, UK). Frozen samples were cut into 14 µm sections using a cryostat (Hyrax C60, Germany), and incubated with primary antibodies Iba1 (1:1500, Cat# NCNP24, Wako Pure Chemical Industries, Japan) and calretinin (1:400, Cat# ab92341, Abcam, USA) overnight in a humidified chamber. Sections were washed with 1x PBS and incubated in the dark for 1 h in a humid environment with appropriate Alexa Fluor® conjugated secondary antibodies (1:400, Alexa Fluor® 488 and Alexa Fluor® 568, Invitrogen, USA). IHC sections were counter-stained with Hoechst (0.1 mg mL^{-1}, Cat# 33258, Sigma Aldrich, Australia), and imaged using a confocal microscope (Zeiss LSM800, Germany). The number of activated microglial cells (Iba1 staining) was determined within a 1.25 mm^2 rectangle, centered on implanted ENMs at weeks 1 and 4, and rosettes in sham operated controls. Thickness of the outer nuclear layer (ONL) was determined by measuring the distance between the inner and outer margins of the ONL, and by counting the number of rows of cell bodies in the ONL. Thickness measurements were done in three sections (left, middle and right) directly above implanted ENMs at weeks 1 and 4 (n = 10) and sham operated controls (n = 6), and then averaged.

2.6 Statistical analysis

Numerical data generated is presented as mean ± standard error (SE), and analyzed using IBM SPSS Version 24 (IBM, USA). Results were compared statistically amongst different groups at each time point using repeated measures ANOVA with Fisher's least significant difference (LSD) *post-hoc* test. Results were also compared between experimental groups at different time points using two-way analysis of variance and Fisher's LSD *post-hoc* test. For all statistical tests significance was associated with $p < 0.05$.

3. Results and discussion

3.1 Polymer properties

Monomer compositions for PLGA and PLDLA were obtained from data sheets provided by Corbion. M_n, PDI and thermal properties of polymers are listed in Table 3. All polymers investigated in this study exhibited M_n > 100 kDa. High M_n ensured a T_g > 37 °C, except for PCL, which is known to have a low T_g [32] (Table 3). PLLA recorded the highest T_g and T_m, while PCL recorded the highest X_c. PLGA and PLDLA recorded low X_c and T_m compared to PLLA due to copolymerization of L-lactide with glycolide and D,L-lactide. These results

are in accordance with published literature [33,34]. Studies have shown polyesters that possess M_n > 100 kDa, coupled with high thermal properties, exhibited slow hydrolytic degradation (> 12 months) [30,31,33-35], which in our case is desirable as this would lead to negligible acid accumulation within the subretinal space, and also preserve the microarchitecture of the biomimetic-like ENMs, aiding RPE cells to form a functional monolayer. Further, the high M_n enabled formation of ENMs on the nanometer scale, described in the next section.

3.2 Evaluation of ENM properties

3.2.1 Physiochemical properties of ENMs

SEM images (Figure 1A-1D) confirmed successfully fabrication of defect-free, randomly aligned non-woven ENMs. All ENMs exhibited a tight fibre distribution (Figure 1A'-1D'), and an average fibre diameter ≤ 70 nm (Table 4). These results are similar to the physical characteristics of the collagen fibres that constitute the ICL [1,6], thereby mimicking the RPE cell supporting layer of native human BM. Average thicknesses of ENMs were close to 1 μm (Table 4 and Figure 1A"-1D"), one quarter that of native human BM [1,6], giving us enough leeway to increase the thickness of ENMs, if required for clinical applications. Average porosities of ENMs determined from SEM images were > 45% (Table 4). The porous nature of the ENMs makes them permeable, which will facilitate exchange of nutrients and metabolites, required for a healthy, polarized RPE monolayer [3]. These consistent physical parameters of the ENMs, matching the physical parameters of the ICL were achieved by optimizing the electrospinning process for each of the polymers investigated in this study (Table 1).

From the topography images (Figure 2), surface roughness (RMS) for ENMs were determined to be > 250 nm (Table 4), significantly higher compared to other substrates, both electrospun membranes and films used as scaffolds for RPE cells [36,37]. The high RMS of our ENMs was a result of the 70 nm electrospun fibre building blocks, which could help mirror the ICL, and also increase laminin adsorption [38-40], positively influencing RPE cell attachment and monolayer formation [3,4,9].

PCL ENMs recorded a low ($p < 0.05$) contact angle measurement compared to PLLA ENMs (Table 4). Contact angle measurements indicate PCL was the least hydrophobic membrane, followed by PLGA and PLDLA, while PLLA was the most hydrophobic. The hydrophobic nature of PLLA ENMs is due to its chemical structure, particularly the presence of pendant methyl groups, which in turn increases its tacticity (stereochemistry) and X_c (38%) [30,35]. Furthermore, surface roughness can also increase observed contact angles measurements for polymer surfaces, when RMS is < 0.1 μm and equilibrium contact angle > 86 ° [41], possibly accounting for our high contact angle measurements. Nevertheless, wettability of ENMs is an important physical parameter as it can directly influence the ability of ENMs to adsorb and maintain laminin on its surface, which in turn influences RPE cell attachment, spreading and monolayer formation [22-24].

Surface stiffness of ENMs is influenced by geometry and polymer properties. In this study ENMs were designed to mimic the ICL, possessing a similar topography and surface roughness (Table 4). Surface stiffness was therefore influenced by the intrinsic properties of the polymers, with PLDLA and PLLA ENMs exhibiting the highest ($p < 0.05$) values. High surface stiffness for PLDLA and PLLA ENMs is due to the presence of L-

lactide in the polymer (Table 3), where increasing amounts of L-lactide increase T_g, T_m and X_c [34,35], in turn increasing stiffness. The stiffness of PLDLA and PLLA ENMs were significantly higher compared to other synthetic BMs [14], and significantly lower compared to collagen based BMs [16].

The modulus of PLLA ENMs was found to be significantly higher ($p < 0.05$), compared to all other ENMs investigated in this study, and also significantly higher compared to the reported moduli of other synthetic scaffolds [37,42], but significantly lower compared to collagen based BMs [16] used to support RPE cells. There is a lack of good data pertaining to the mechanical properties of native BM, and no data pertaining to the mechanical properties of the ICL, primarily because it is hard to source young, healthy tissue. Chan et al., [43] estimated the modulus of native BM to be 7 - 19 MPa from four donors aged 22, 31, 75 and 83 years. This data lacks sufficient power to extrapolate statistical analysis, making it hard to compare with our ENMs. The high modulus of PLLA ENMs, like surface stiffness is due its high X_c and high M_n, coupled with its stereochemistry [34,35], which in turn increased its modulus. The surface stiffness and modulus of ENMs are important physical parameters, directly influencing the conformation of adsorbed laminin [25,26], in turn influencing RPE cell attachment, and monolayer formation, and also directly influencing cell fate [27-29].

3.2.2 Laminin adsorption on ENMs

Laminin, an extracellular protein is synthesized by RPE cells, and is found lining the top of the ICL [6,20,44,45]. Human BMs contain laminin-521, laminin-511, laminin-332 and laminin-111 [44]. Aisenbrey et al., [44] showed laminin-111 and -332 promoted RPE cell attachment and maturation, while laminin-511 and -521 encouraged migration. Researchers have investigated the use of various xeno-free protein coatings, and their importance on different RPE cells particularly in fabricating functional retinal constructs [3,44-46]. As proof of principle we used mouse laminin, composed largely of laminin-111 [44]. Quantitative measurements showed significantly low ($p < 0.05$) amounts of laminin adsorbed to the controls compared to ENMs (Figure 3), further supported by qualitative, IHC assessments (Figure 3). Several groups have reported high protein adsorption on nano-structured 3D substrates compared to 2D substrates [38-40]. Recently, Hammarin et al., [39] reported that laminin adsorbed significantly more to nanowires than to flat surfaces, primarily due to geometrical effects. The geometry of our ENMs are similar to the geometry of nanowires used in the Hammarin et al., [39] study, which could be the driving force for increased laminin adsorption on the surface of our ENMs.

Laminin adsorption on the surface of ENMs increased with increasing contact angle measurements (Table 4), with PLDLA and PLLA ENMs adsorbing high amounts of laminin (Figure 3). This increased laminin adsorption is driven by the hydrophobic nature of PLDLA and PLLA ENMs [30,35]. In solution, laminin interacts with water molecules to lower its entropy creating a folded structure, where the hydrophobic amino acid side chains (non-polar groups) occupy the interior of the folded protein structure [22-24]. PCL ENMs exhibited the lowest contact angle measurement (Table 4), an indication of its hydrophilic nature compared to PLDLA and PLLA. The relatively hydrophilic interaction between the surface of the PCL ENMs and water molecules may have created a large energy barrier for laminin to overcome to adsorb to PCL ENMs [22-24],

while the hydrophobic interaction between the surfaces of the PLDLA and PLLA ENMs, and water molecules likely created a thermodynamically favourable state apt for increased laminin adsorption [22-24]. Del Priore et al., [20] reported that coating the ICL with 4 $\mu g \cdot cm^{-2}$ of laminin increased RPE attachment, which is similar to our concentrations for PLGA, PLDLA and PLLA based ENMs (Figure 3). The increased adsorption of laminin on PLDLA and PLLA ENMs is encouraging, as laminin is known to mediate RPE cell attachment [20,44,47,48] via integrin β_1 subunits on the RPE cell surface [10].

3.3 *In vitro* studies

3.3.1 SEM images of hRPE cells on ENMs

Figure 4, shows hRPE cells cultured on ENMs and 2D controls (24-well laminin coated tissue culture plates). At week 1, hRPE cells cultured on ENMs were 100% confluent (Figure 4B-4E) compared to 2D controls, which were < 50% confluent (Figure 4A), indicating high cell attachment on ENMs, a vital property for the clinical application of synthetic BMs [3,6,7]. At week 1, hRPE cells cultured on ENMs, exhibited early signs of microvilli formation, particularly on PLLA ENMs (Figure 4E"). At week 2, all conditions exhibited complete RPE monolayers (Figure 4F-4J), but only hRPE cells cultured on 70 nm ENMs exhibited apical microvilli (Figure 4G'-4J' and 4G"-4J"). At week 4, hRPE cells growing on 70 nm ENMs exhibited a mature monolayer (Figure 4L-4O) with a 3D polygonal-cobblestone structure, and a well-formed, dense apical microvilli (Figure 4L'-4O' and 4L"-4O"), compared to hRPE cells cultured on controls (Figure 4K' and 4K"). At week 8, hRPE cells cultured on 2D controls exhibited apical microvilli (Figure 4P' and 4P"); first exhibited at week 2 by hRPE cells cultured on 70 nm ENMs (Figure 4G'-4J' and 4G"-4J"). At week 8, 70 nm ENMs continued to support mature RPE monolayers (Figure 4Q-4T), exhibiting 3D polygonal-cobblestone structure, and dense apical microvilli (Figure 4Q'-4T' and 4Q"-4T"), critical for barrier function, a characteristic of mature RPE monolayers [3,7]. SEM results suggest that laminin coated ENMs are aptly suited for hRPE culture compared to 2D laminin coated surfaces, which is in accordance with published literature [4,14,15,17,36], and that a minimum of four weeks of *in vitro* culture is required for mature hRPE monolayer formation.

The early formation of hRPE monolayers on ENMs can be attributed to increased laminin adsorption, and microenvironments emulating the ICL of native human BM [18,19]. The high surface stiffness and modulus of PLDLA and PLLA ENMs likely caused conformational changes in the adsorbed laminin, leading to increased exposure of laminin cell-binding domains [25,26], creating an ideal surface for hRPE cells to form a mature monolayer. hRPE cells could also be responding to surface mechanical cues, possibly transmitted via mechanotransduction from the surface of PLLA ENMs via focal adhesion sites to integrin receptors present in hRPE cell membranes [27-29]. The SEM results support the need for a biomimetic, nanofibrous scaffold, particularly a laminin coated 70 nm PLLA ENM which is capable of supporting a mature hRPE monolayer with dense apical microvilli, required for effective phagocytosis of shed POS [3,8,9].

3.3.2 hRPE cell proliferation and cytotoxicity of ENMs

The WST-1 cell proliferation reagent is designed for spectrophotometric quantification of cell proliferation, growth, viability, and chemosensitivity to external factors. An increase in viable cells results in an increase in mitochondrial activity, which leads to an increase in the amount of formazan dye formed, directly correlating to the number of metabolically active cells. This assay can therefore be used as a proxy for cell number [15], and valid if metabolic effects of experimental variables are smaller than the effect on cell numbers.

WST-1 results (Figure 5) showed hRPE cells to be metabolically active on all surfaces, indicating laminin coated ENMs supported hRPE cell proliferation. Over the 14 day culture period, PLLA ENMs significantly ($p < 0.05$) promoted hRPE cell proliferation compared to all other conditions. The high metabolic activity of hRPE cells proliferating on 70 nm PLLA ENMs can be attributed to high surface stiffness and modulus, similar to a recent study by White et al., [2] which showed ARPE-19 cells to possess high metabolic activity, and spread more homogenously on high modulus scaffolds. Additionally, increased laminin adsorption (Figure 3), and probable ideal laminin conformation on the surface of PLLA ENMs could have further augmented initial RPE cell adhesion and proliferation [25,26]. These results, coupled with the SEM results (Figure 4), validate the ability of ENMs to support hRPE cell metabolism and proliferation, and hence non-cytotoxic to RPE cells.

3.3.3 TER of hRPE monolayers on ENMs

hRPE cells cultured on ENMs first exhibited TER values at week 1, at the onset of RPE monolayer formation determined via light microscopy. Thereafter TER increased with time through week 8 (Figure 6), indicative of tight junction formation within a confluent RPE monolayer, where confluency is supported by SEM images (Figure 4). At weeks 1 and 2, hRPE monolayers cultured on PLDLA and PLLA ENMs exhibited significantly higher ($p < 0.05$) TER values compared to those cultured on PCL and PLGA (Figure 6). At weeks 3, 4 and 8, hRPE monolayers cultured on PLLA ENMs exhibited the highest ($p < 0.05$) TER values (Figure 6). At week 3, hRPE monolayers cultured on PLLA ENMs recorded a TER of 200 $\Omega \cdot cm^2$, similar to TER recorded for hRPE cells *in situ* [49,50], which further increased to 270 $\Omega \cdot cm^2$ at week 8 (Figure 6). Increase in TER with time, particularly for hRPE cells cultured on PLLA ENMs, indicates tight junction formation, a characteristic functional attribute of mature RPE monolayers [3,50], and is likely due to its high modulus and biomimetic-like nature [18,19]. These results strongly demonstrate the ability of PLLA ENMs to support RPE monolayers and barrier function over long-term culture.

3.3.4 Gene expression of hRPE monolayers on ENMs

To further study suitability of ENMs as scaffolds for retinal cells, gene expression of hRPE cells cultured on ENMs was performed. PMEL17 a marker of mature RPE cells regulates and is expressed in association with melanogenesis [51,52]. ZO1 assists in formation of multi-protein complexes at cytoplasmic surfaces of intercellular junctions, tight junctions, and is a marker of RPE cell monolayers [53,54]. BEST1 a RPE membrane protein regulates both, chloride and Ca^{2+} channels [53,55]. RPE65 is a mature RPE protein required

for cis-trans isomerization of retinol in the RPE-photoreceptor vitamin A cycle [53,56]. RPE cells secrete PEDF and VEGF preferably from their apical and basal surfaces, respectively [53,57]. PEDF is neurotrophic and anti-angiogenic, and low levels of PEDF in the RPE basal region can prevent neovascularization [57]. VEGF is necessary for maintenance of endothelial cells in the choriocapillaris [57], and an increase in its critical threshold concentration will induce neovascularization [57]. RPE cells phagocytose shed POS daily, and activation of MerTK and LAMP2 in RPE cells is critical for efficient engulfment and processing of shed POS [53,58].

In this study, hRPE cells cultured in 24-well, laminin coated tissue culture plates at week 2 served as controls, and the results in Figure 7 are presented as fold-change normalized to week 2 controls. The results demonstrated that hRPE monolayers cultured on laminin coated ENMs expressed all RPE genes as early as week 2, after which their expressions significantly increased. At week 4, there were significant increases ($p < 0.05$) in expressions of PMEL17, ZO1, BEST1, PEDF and VEGF compared to week 2 (Figure 7A, 7B, 7C, 7E and 7F). Although not statistically significant increased expressions were observed for RPE65, MerTK and LAMP2 at week 4, compared to week 2. At week 8, hRPE cells cultured on ENMs and controls exhibited significant increases ($p < 0.05$) for all RPE genes compared to weeks 2 and 4 (Figure 7A-7H). Even though there are some significant differences in gene expression between the four ENMs at specific time points, it is difficult to say with certainty, based on qPCR results alone, that a particular type of polymer based ENM is best suited for hRPE cells. The increased expression and maintenance of RPE genes over long-term culture however, suggests that hRPE cells attached, proliferated and formed functional monolayers on all ENMs.

In accordance with results for hRPE cell attachment and proliferation, and TER, the long-term expression of signature RPE genes is possibly due to the construction of a synthetic, laminin coated, biomimetic-like ICL mimicking the RPE cell supporting layers [18,19] of the BM. The gene expression of growth factors points to the possible potential of ENMs being able to support a RPE monolayer characterized with polarized secretion of VEGF and PEDF, required for the maintenance of a healthy retina [57]. Future *in vitro* experiments using Transwells™ will quantify concentration and secretion polarity of PEDF and VEGF for RPE monolayers cultured on ENMs, which will add to the utility of 70 nm ENMs as scaffolds for retinal cells.

3.3.5 IHC assessment of hRPE monolayers on ENMs

At week 2, controls (laminin coated tissue culture treated coverslips) and laminin coated 70 nm ENMs stained positive for signature RPE markers. Positive staining of Cytokeratin18 (Figure 8A-8E) at week 2 showed ENMs preserving the epithelia phenotype of hRPE cells [59], while nuclear expression of Ki67 (Figure 8A-8E) showed ENMs supported hRPE cell proliferation [60], leading to hRPE monolayers at week 2. Further, at week 2, ZO1 was expressed (Figure 8F-8J) at the intercellular membrane, and within the hRPE cell cytoplasm and nucleus, where it is synthesized and later transported to intercellular membranes, indicative of maturing RPE monolayers [53,54]. The early (week 2) positive nuclear staining of MITF, which controls the expression of genes essential for normal melanin synthesis (Figure 8K-8O) is further indicative of RPE linage specificity [53].

At week 4, Cytokeratin18 staining (Figure 8A'-8E') for both controls and ENMs were significantly obscured by the presence of melanin in the apical cytoplasm. Expression of Cytokeratin18 however, confirmed that ENMs preserved and maintained RPE epithelia phenotype. The absence of Ki67 at week 4, suggested a halt in hRPE cell proliferation [60] (Figure 8A'-8E'). At week 4, positive ZO1 staining (Figure 8F'-8J') at the intercellular membrane is reminiscent of mature RPE monolayers [53,54], particularly in hRPE cells cultured on PLLA (Figure 8J') and PLDLA (Figure 8I') ENMs. At week 4, MITF was expressed and localized in the nuclei of hRPE cells cultured on ENMs (Figure 8K'-8O'), further confirming lineage specificity [53].

At week 8, continued Cytokeratin18 expression (Figure 8A"-8E") confirmed ENMs could preserve RPE epithelial phenotype in long-term culture. As with week 4, there was no expression of Ki67 at week 8 (Figure 8A"-8E"). Continued ZO1 staining at week 8 (Figure 8F"-8J") ratifies the ability of EMNs to maintain mature RPE monolayers. Expression of ZO1 was particularly high in hRPE cells cultured on PLLA (Figure 8J") and PLDLA (Figure 8I") ENMs, which exhibited tightly formed hRPE monolayers with characteristic polygonal RPE cell structures [3,4,9]. As with week 4, there was continued expression and localization of MITF in the nuclei of hRPE cells at week 8 (Figure 8K"-8O") confirming lineage specificity [53].

At week 8, hRPE cells cultured on ENMs and control stained positive for MCT1 (Figure 8P"-8T"). Proper localization of MCT1 at the apical surface [61] for hRPE cells cultured on ENMs demonstrates that these cells are actively involved in the transport of lactate and pyruvate required for maintenance of a healthy retina [61]. Further, at week 8, hRPE cells cultured on controls and ENMs stained positive for MerTK (Figure 8U"-8Y"), required for efficient engulfment and processing of shed POS [58]. Expression of MerTK was evenly distributed and localized in the cytoplasm for hRPE cells cultured on ENMs, particularly PLLA (Figure 8Y") and PLDLA (Figure 8X") ENMs, which could lead to these cells possessing a high phagocytic activity.

Counter staining with DAPI showed hRPE cell nuclei were centrally located with no overlapping, supporting our claim of hRPE monolayer formation on ENMs. The presence of signature RPE markers in expected temporal and spatial locations assessed by IHC, supports the qPCR results, and indeed compliments results obtained for hRPE cell attachment and proliferation, SEM, and TER, and can be credited to the creation of biomimetic-like scaffolds that resembles the RPE cell supporting layers [18,19] of native human BM.

3.3.6 Phagocytic capability of hRPE cells cultured on ENMs

The capacity of RPE cells to phagocytose shed POS is a vital physiological function necessary for maintenance of healthy and functional photoreceptors [3,7,9]. At week 8, results showed hRPE cells cultured on all ENMs and controls to phagocytose, confirmed by digestion of polystyrene latex beads and positive expression of MerTK (Figure 9A-9E). We acknowledge beads are not the best substitute for POS to evaluate RPE cell phagocytosis, and are only used as supporting evidence for functional and molecular assays, including TER (Figure 6), qPCR (Figure 7) and IHC (Figure 8). To overcome the limitation of the beads, phagocytosing hRPE cells were stained for MerTK, a gene turned on during phagocytosis of shed POS [53,58]. MerTK expression was found in both the cytoplasm and nucleus for all conditions, when hRPE monolayers were

disrupted with trypsin and re-seeded as single cells (Figure 9A-9E), which otherwise is specifically localized in the cytoplasm [58] (Figure 8U"-8Y"). The co-localization of MerTK in the cytoplasm and nucleus in single hRPE cells maybe because they reverted to partial immaturity when trypsinized.

hRPE cells cultured on PLLA ENMs, which exhibited the highest modulus (48 MPa, Table 4), ingested significantly more beads per cell compared to all the other conditions, and also exhibited the highest percentage of phagocytosing cells (Figure 9F). FAK has been shown to play an important role in MerTK activation, thereby influencing RPE cell phagocytosis [58,62]. Activation of FAK in RPE cells is directly triggered by integrins involved in cytoskeletal reorganization [58,62]. hRPE monolayers cultured on PLLA ENMs may have undergone cytoskeletal reorganization, activating FAK, in turn activating MerTK, thereby increasing its phagocytic capacity. Our results are contrary to the study by Boochoon et al., [63] where ARPE-19 cells exhibited decreased phagocytosis when grown on gels possessing a high elastic modulus. These gels, however, were non-porous [63], and did not mimic the RPE cell supporting layers of the BM. Mimicking the native extra-cellular matrix (ECM), particularly for retinal constructs is an important design criteria, as it is well established that scaffold microenvironment, coupled with its mechanical properties dictates cellular function [18,19]. The absence of a native-like microenvironment in the study conducted by Boochoon et al., [63] might have caused ARPE-19 cells to exhibit decreased phagocytic activity when cultured on firm gels. Additionally, high laminin adsorption augmented by the possibility of ideal laminin conformation on the surface of PLLA ENMs [25,26], could have caused hRPE cells investigated in our study to exhibit increased phagocytic activity.

The human fovea is responsible for sharp central vision, and is packed with *ca.* 30 cones per RPE cell [64], requiring each RPE cell to phagocytosis *ca.* 30 shed POS daily. hRPE cells cultured on laminin coated 70 nm PLLA ENMs ingested 101 ± 11 beads per cell, which is significantly more ($p < 0.05$) compared to all the other conditions (Figure 9F), and well above the physiological requirement of healthy RPE cells in the fovea. This increased phagocytic activity for hRPE cells cultured on 70 nm PLLA ENMs is supported by significantly high ($p < 0.05$) gene expression of MerTK (Figure 7G) and LAMP2 (Figure 7H), critical for efficient processing of shed POS [58,62], coupled with consistent and localized distribution of MerTK in the cytoplasm of mature hRPE monolayers grown on PLLA ENMs (Figure 8Y"). These results further substantiate the ability of laminin coated 70 nm PLLA ENMs to support functional hRPE monolayers over long-term culture.

3.3.7 TEM images of hRPE monolayers on PLLA ENMs

From the *in vitro* results, it is clear that laminin coated 70 nm PLLA ENMs were best suited for hRPE cells, which were further assessed using TEM. At week 4, TEM images confirmed a healthy and mature hRPE monolayer on the surface of PLLA ENMs (Figure 10A), including apical microvilli (MV, Figure 10A and 10A'), and basal infoldings (IF, Figure 10A"), characteristic of native RPE cells. At week 4, TEM images (Figure 10A, 10A' and 10A") confirmed the presence of smooth (SER), and rough endoplasmic reticulum (RER), cytoplasmic mitochondria (CM), and cell nucleus (CN). At week 8, hRPE cells cultured on PLLA ENMs continued to exhibit apical microvilli (Figure 10B and 10B') and basal infoldings (Figure 10B") characteristic of native RPE cells,

coupled with cellular organelles as seen in week 4 (Figure 10), and is in accordance with published literature [3,5,46]. Unlike Pilgrim et al., [65] our TEM results did not show focal and diffuse deposits containing lipids, proteins or calcium. hRPE cells used in our study were passage 3, this coupled with 8 weeks of culture might have impeded deposit formation. If deposits accumulated with increased culture time, we hypothesis the porous nature of our ENMs may allow most deposits to flow through it and into the culture media, which will be confirmed in future studies. Importantly, the TEM results coupled with all the *in vitro* results supports our hypothesis that the combined effects of laminin, optimal mechanical properties and the creation of a synthetic, biomimetic-like ICL will positively influence hRPE cells to form a functional, native-like monolayer.

3.4 *In vivo* studies

3.4.1 Subretinal implantation of PLLA ENMs

To test biocompatibility, we developed a surgical technique to reproducibly implant only PLLA ENMs flat into the subretinal space of *rdy* rats. To this effect, 10 μm PLLA ENMs were encapsulated in 20 w/v% gelatin, cooled at 4 °C for 5 min, and then cut into 0.8 mm discs. The gelatin encapsulating the ENMs hardened when cooled, increasing the rigidity and improving handling, while the circular shape of the ENMs helped reduce tissue damage during subretinal implantation. At 37 °C (internal body temperature) the gelatin dissolved and was cleared, leaving only PLLA ENMs within the subretinal space. At week 1, fundus imaging and OCT scans showed the implanted laminin coated PLLA ENMs (Figure 11A and 11A') were stable for conformation and location within the subretinal space. Retinal integrity was assessed from both OCT images (Figure 11A') and H&E sections (Figure 11C and 11D), which showed mild disruption of the retinal structures due to implantation of PLLA ENMs, compared to sham operated controls (Figure 11B). In summary, the surgical technique we developed resulted in successful and reproducible implantation of PLLA ENMs, flat within the subretinal space of *rdy* rats, similar to surgical techniques developed in previous studies [17,66,67].

3.4.2 Biocompatibility of PLLA ENMs

To evaluate biocompatibility of PLLA ENMs, including the laminin coating and sandwiching gelatin, sections of sham operated controls, and implanted eyes were assessed histologically via H&E, and immunofluorescence for Iba1 (red), calretinin (green) and Hoechst (blue) at weeks 1 and 4, post-implantation. Hoechst and calretinin were used to assess the structure of the retina, where Hoechst was used to stain cell nuclei in the outer (ONL) and inner nuclear (INL) layers, while calretinin was used as a marker for amacrine and ganglion cell bodies, as well as their processes in the inner plexiform layer (IPL) and ganglion cell layer (GCL).

10 μm thick PLLA ENMs were used in the *in vivo* study, which are 2 fold thicker than native human BM (5 μm thick [6,7]), ensuring they were implanted flat in the subretinal space. The space limitation of the subretinal space requires retinal scaffolds to be thin (5 - 90 μm [8]), which our PLLA ENMs are making them clinically viable. Within the subretinal space, based on Vroman Effect [68] the laminin coating could be desorbed and replaced by less motile proteins that have an affinity for PLLA. Alternatively, in the absence of

immunosuppressants given enough time the invading microglial cells could remodel the laminin coating. The high M_n PLLA used undergoes slow hydrolytic degradation [30,31,33-35], and *in vivo* this could account for negligible acid accumulation, thereby preserving the porosity of the implanted PLLA ENMs. In AMD patients, treated with a tissue-engineered retinal construct, we hypothesize the overlaying RPE cells could synthesize their own ECM, which in turn could support the overlaying retinal cells, and takeover from the degrading PLLA ENM [18]. Unlike the study by Stanzel et al., [69], our *in vivo* studies using PLLA ENMs only did not show retinal destruction (Figure 11). Furthermore, *in vitro* studies showed gelatin dissolved in 30 min without negatively affecting hRPE monolayers (data not shown). This non-inflammatory response could be due to gelatin's thermoresponsive property [69], and the low volume used to encapsulate the PLLA ENMs, causing it to be cleared fast from within the subretinal space.

Microglial cells are normally confined to inner retinal layers where they perform maintenance and immunological roles [17,67]. Biocompatibility studies typically use immunosuppressants to counter the effect of microglial activation [15,17], which masks the true measure of biocompatibility. It is important to acknowledge our biocompatibility study was done in the absence of immunosuppressants, and that PLLA ENMs were implanted trans-sclerally, damaging the outer and inner retina, thereby compromising the immune-privilege of the *rdy* rat's eye. As seen in H&E sections, immunofluorescent staining also exhibited retinal disruption due to implanted PLLA ENMs, similar to sham operated controls (Figure 11B'-11D'). Further, at weeks 1 and 4 post-implantation whorls and rosettes were exhibited (Figure 11C'-11D'), which is a typical reaction when connections between POS and RPE cells are interrupted.

Inflammatory responses to implanted PLLA ENMs were assessed via immunofluorescent staining of microglial cells using ionized Ca2+ binding adapter molecule-1 (Iba1). Iba1 staining showed microglial response at weeks 1 and 4, post-implantation of PLLA ENMs (Figure 11C'-11D'), caused by compromising the immune-privilege of the rat's eye, in turn leading to immediate microglial activation, proliferation and migration [17,67] towards the implanted PLLA ENM. Interestingly, the number of activated microglial cells significantly dropped ($p < 0.05$) at week 4 compared to week 1, and was similar to sham operated controls (Figure 11B' - 11D' and Figure 11E). A study by Antognazza et al., [67] showed microglial activation to drop to a level similar to sham operated controls after 5 months, while our study showed a significant drop at week 4, indicating the possible biocompatibility of the laminin coated PLLA ENMs within the subretinal space. Recently, Koss et al., [70] implanted retinal constructs subretinally in Yucatán pig eyes, using an intravitreal surgical approach. In humans, this surgical approach coupled with the administration of immunosuppressants, may not induce strong microglial activation and migration towards an implanted retinal construct aimed at treating dry AMD.

At week 1, post-implantation of PLLA ENMs no significant decrease ($p < 0.05$) in ONL thickness was observed compared to sham operated controls (Figure 11F), which could be due to trans-implant nutrient transport, supported by the porous nature of the ENM, a vital design characteristic for retinal scaffolds [3,8]. At week 4, a significant decrease ($p < 0.05$) in ONL thickness was observed (Figure 11F), which compared to other studies [15,17,67] show a complete loss of the ONL at week 4. ONL thinning occurred at the distal end above

the implanted PLLA ENMs and away from the insertion site, primarily caused due to interruptions between the ONL and RPE cells by implanted ENMs. The *in vivo* results, coupled with *in vitro* results validates the use of porous, laminin coated 70 nm PLLA ENMs as a scaffold in the fabrication of cell-loaded retinal constructs.

4. Conclusion

Synthetic, ENMs with average fibre diameters ≤ 70 nm, the first of their kind reported in literature as scaffolds for RPE cells, with thicknesses *ca.* 1 μm and porosities > 45%, were successfully fabricated from PCL, PLGA, PLDLA and PLLA, and coated with laminin to mimic the RPE cell supporting layers of native human BM. We found laminin coated 70 nm PLLA ENMs not only accelerated hRPE cell proliferation, but also promoted the formation of a functional hRPE monolayer on its surface. 10 μm thick, laminin coated 70 nm PLLA ENMs were successfully implanted into the subretinal space of *rdy* rats, which at week 4 in the absence of immunosuppressants were surrounded by a significantly low number of activated microglial cells compared to week 1, with no adverse immune response, and a thin yet distinctive ONL. In conclusion, porous laminin coated 70 nm PLLA ENMs are therefore suitable scaffolds to support functional hRPE monolayers. Future work will focus on developing a tissue-engineered retinal construct, comprising human embryonic stem cell derived retinal cells supported by PLLA ENM aimed at treating dry AMD.

Acknowledgements

This research project was funded by the Clem Jones Foundation in Brisbane, Queensland, Australia. Part of the physiochemical assessments of ENMs was performed in collaboration with the Queensland Node of Australian National Fabrication Facility (ANFF), a company established under the National Collaborative Research Infrastructure Strategy to provide nano and microfabrication facilities for Australia's researchers. We wish to thank Mr. Gene Venables, Department of Anatomy and Neuroscience, The University of Melbourne, for his technical assistance with this project.

References

[1] P. Fernández-Robredo, A. Sancho, S. Johnen, S. Recalde, N. Gama, G. Thumann, J. Groll, A. García-Layana, Current Treatment Limitations in Age-Related Macular Degeneration and Future Approaches Based on Cell Therapy and Tissue Engineering, J Ophthalmol. 2014 (2014) 1–13. doi:10.1155/2014/510285.

[2] C. White, T. DiStefano, R. Olabisi, The influence of substrate modulus on retinal pigment epithelial cells, J Biomed Mater Res A. 105 (2017) 1260–1266. doi:10.1002/jbm.a.35992.

[3] N.A. Hotaling, V. Khristov, Q. Wan, R. Sharma, B.S. Jha, M. Lotfi, A. Maminishkis, C.G. Simon, K. Bharti, Nanofiber Scaffold-Based Tissue-Engineered Retinal Pigment Epithelium to Treat Degenerative Eye Diseases, J Ocul Pharmacol Ther. (2016). doi:10.1089/jop.2015.0157.

[4] B.S. Jha, K. Bharti, Regenerating Retinal Pigment Epithelial Cells to Cure Blindness: A Road Towards Personalized Artificial Tissue, Curr Stem Cell Rep. 1 (2015) 79–91. doi:10.1007/s40778-015-0014-4.

[5] A.M.A. Shadforth, S. Suzuki, C. Theodoropoulos, N.A. Richardson, T.V. Chirila, D.G. Harkin, A Bruch's membrane substitute fabricated from silk fibroin supports the function of retinal pigment epithelial cells in vitro, J Tissue Eng Regen Med. (2015). doi:10.1002/term.2089.

[6] J.C. Booij, D.C. Baas, J. Beisekeeva, T.G.M.F. Gorgels, A.A.B. Bergen, The dynamic nature of Bruch's membrane, Prog Retin Eye Res. 29 (2010) 1–18. doi:10.1016/j.preteyeres.2009.08.003.

[7] C.A. Curcio, M. Johnson, Chapter 20 - Structure, Function, and Pathology of Bruch's Membrane, in: S.J. Ryan, S.R. Sadda, D.R. Hinton, A.P. Schachat, S.R. Sadda, C.P. Wilkinson, P. Wiedemann, A.P. Schachat (Eds.), Retina (Fifth Edition), W.B. Saunders, London, 2013: pp. 465–481.

[8] S.R. Hynes, E.B. Lavik, A tissue-engineered approach towards retinal repair: scaffolds for cell transplantation to the subretinal space, Graefes Arch. Clin. Exp. Ophthalmol. 248 (2010) 763–778. doi:10.1007/s00417-009-1263-7.

[9] K. Bharti, M. Rao, S.C. Hull, D. Stroncek, B.P. Brooks, E. Feigal, J.C. van Meurs, C.A. Huang, S.S. Miller, Developing cellular therapies for retinal degenerative diseases, Invest. Ophthalmol. Vis. Sci. 55 (2014) 1191–1202. doi:10.1167/iovs.13-13481.

[10] T.C. Ho, L.V. Del Priore, Reattachment of cultured human retinal pigment epithelium to extracellular matrix and human Bruch's membrane, Invest. Ophthalmol. Vis. Sci. 38 (1997) 1110–1118.

[11] T.H. Tezel, H.J. Kaplan, L.V. Del Priore, Fate of human retinal pigment epithelial cells seeded onto layers of human Bruch's membrane, Invest. Ophthalmol. Vis. Sci. 40 (1999) 467–476.

[12] T.H. Tezel, L.V. Del Priore, Repopulation of different layers of host human Bruch's membrane by retinal pigment epithelial cell grafts, Invest. Ophthalmol. Vis. Sci. 40 (1999) 767–774.

[13] G.R. Da Silva, T.H. Lima, R.L. Oréfice, G.M. Fernandes-Cunha, A. Silva-Cunha, M. Zhao, F. Behar-Cohen, In vitro and in vivo ocular biocompatibility of electrospun poly(ε-caprolactone) nanofibers, Eur J Pharm Sci. 73 (2015) 9–19. doi:10.1016/j.ejps.2015.03.003.

[14] Š. Popelka, H. Studenovská, L. Abelová, T. Ardan, P. Studený, Z. Straňák, J. Klíma, B. Dvořánková, J. Kotek, J. Hodan, F. Rypáček, A frame-supported ultrathin electrospun polymer membrane for transplantation of retinal pigment epithelial cells, Biomed Mater. 10 (2015) 045022. doi:10.1088/1748-6041/10/4/045022.

[15] P. Xiang, K.-C. Wu, Y. Zhu, L. Xiang, C. Li, D.-L. Chen, F. Chen, G. Xu, A. Wang, M. Li, Z.-B. Jin, A novel Bruch's membrane-mimetic electrospun substrate scaffold for human retinal pigment epithelium cells, Biomaterials. 35 (2014) 9777–9788. doi:10.1016/j.biomaterials.2014.08.040.

[16] P.H. Warnke, M. Alamein, S. Skabo, S. Stephens, R. Bourke, P. Heiner, Q. Liu, Primordium of an artificial Bruch's membrane made of nanofibers for engineering of retinal pigment epithelium cell monolayers, Acta Biomater. 9 (2013) 9414–9422. doi:10.1016/j.actbio.2013.07.029.

[17] Z. Liu, N. Yu, F.G. Holz, F. Yang, B.V. Stanzel, Enhancement of retinal pigment epithelial culture characteristics and subretinal space tolerance of scaffolds with 200 nm fiber topography, Biomaterials. 35 (2014) 2837–2850. doi:10.1016/j.biomaterials.2013.12.069.

[18] P.X. Ma, Biomimetic materials for tissue engineering, Advanced Drug Delivery Reviews. 60 (2008) 184–198. doi:10.1016/j.addr.2007.08.041.

[19] J. Kim, H.N. Kim, Y. Lang, A. Pandit, Biologically inspired micro- and nanoengineering systems for functional and complex tissues, Tissue Eng Part A. 20 (2014) 2127–2130. doi:10.1089/ten.tea.2013.0707.

[20] L.V. Del Priore, L. Geng, T.H. Tezel, H.J. Kaplan, Extracellular matrix ligands promote RPE attachment to inner Bruch's membrane, Curr. Eye Res. 25 (2002) 79–89.

[21] F. von Burkersroda, L. Schedl, A. Göpferich, Why degradable polymers undergo surface erosion or bulk erosion, Biomaterials. 23 (2002) 4221–4231. doi:10.1016/S0142-9612(02)00170-9.

[22] C.A. Haynes, W. Norde, Globular proteins at solid/liquid interfaces, Colloids Surf B Biointerfaces. 2 (1994) 517–566. doi:10.1016/0927-7765(94)80066-9.

[23] J. Vitte, A.M. Benoliel, A. Pierres, P. Bongrand, Is there a predictable relationship between surface physical-chemical properties and cell behaviour at the interface? Eur Cell Mater. 7 (2004) 52–63.

[24] C.J. Wilson, R.E. Clegg, D.I. Leavesley, M.J. Pearcy, Mediation of biomaterial-cell interactions by adsorbed proteins: a review, Tissue Eng. 11 (2004) 1–18. doi:10.1089/ten.2005.11.1.

[25] M.C. Vyner, L. Liu, H.D. Sheardown, B.G. Amsden, The effect of elastomer chain flexibility on protein adsorption, Biomaterials. 34 (2013) 9287–9294. doi:10.1016/j.biomaterials.2013.08.086.

[26] J.-H. Seo, K. Sakai, N. Yui, Adsorption state of fibronectin on poly(dimethylsiloxane) surfaces with varied stiffness can dominate adhesion density of fibroblasts, Acta Biomater. 9 (2013) 5493–5501. doi:10.1016/j.actbio.2012.10.015.

[27] J. Barthes, H. Özçelik, M. Hindié, A. Ndreu-Halili, A. Hasan, N.E. Vrana, Cell microenvironment engineering and monitoring for tissue engineering and regenerative medicine: the recent advances, Biomed Res Int. 2014 (2013) 921905–921905. doi:10.1155/2014/921905.

[28] J.K. Carrow, A.K. Gaharwar, Bioinspired Polymeric Nanocomposites for Regenerative Medicine, Macromol. Chem. Phys. 216 (2014) 248–264. doi:10.1002/macp.201400427.

[29] J. Eyckmans, T. Boudou, X. Yu, A Hitchhiker's Guide to Mechanobiology, Developmental Cell. 21 (2011) 35–47. doi:10.1016/j.devcel.2011.06.015.

[30] E.W. Fischer, H.J. Sterzel, G. Wegner, Investigation of the structure of solution grown crystals of lactide copolymers by means of chemical reactions, Kolloid-Z.U.Z.Polymere. 251 (1973) 980–990. doi:10.1007/BF01498927.

[31] C.G. Pitt, F.I. Chasalow, Y.M. Hibionada, D.M. Klimas, A. Schindler, Aliphatic polyesters. I. The degradation of poly(ϵ-caprolactone) in vivo, J. Appl. Polym. Sci. 26 (1981) 3779–3787. doi:10.1002/app.1981.070261124.
[32] C.A. Harper, Modern Plastics Handbook, McGraw-Hill. (2000) 1–1298.
[33] E. Ruckenstein, Y. Yuan, Molten ring-open copolymerization of L-lactide and cyclic trimethylene carbonate, J. Appl. Polym. Sci. 69 (1998) 1429–1434. doi:10.1002/(SICI)1097-4628(19980815)69:7<1429::AID-APP18>3.0.CO;2-O.
[34] D.C. Surrao, S.D. Waldman, B.G. Amsden, Biomimetic Poly(Lactide) Based Fibrous Scaffolds for Ligament Tissue Engineering, Acta Biomater. 8 (2012) 3997–4006. doi:10.1016/j.actbio.2012.07.012.
[35] R.A. Auras, L.T. Lim, S.E.M. Selke, H. Tsuji, Poly(lactic acid): Synthesis, Structures, Properties, Processing, and Applications, John Wiley & Sons, Inc, 2011.
[36] A. Sorkio, P.J. Porter, K. Juuti-Uusitalo, B.J. Meenan, H. Skottman, G.A. Burke, Surface Modified Biodegradable Electrospun Membranes as a Carrier for Human Embryonic Stem Cell-Derived Retinal Pigment Epithelial Cells, Tissue Eng Part A. 21 (2015) 2301–2314. doi:10.1089/ten.TEA.2014.0640.
[37] S. Suzuki, R.A. Dawson, T.V. Chirila, A.M.A. Shadforth, T.A. Hogerheyde, G.A. Edwards, D.G. Harkin, Treatment of Silk Fibroin with Poly(ethylene glycol) for the Enhancement of Corneal Epithelial Cell Growth, J Funct Biomater. 6 (2015) 345–366. doi:10.3390/jfb6020345.
[38] A. Dolatshahi-Pirouz, T. Jensen, D.C. Kraft, M. Foss, P. Kingshott, J.L. Hansen, A.N. Larsen, J. Chevallier, F. Besenbacher, Fibronectin adsorption, cell adhesion, and proliferation on nanostructured tantalum surfaces, ACS Nano. 4 (2010) 2874–2882. doi:10.1021/nn9017872.
[39] G. Hammarin, H. Persson, A.P. Dabkowska, C.N. Prinz, Enhanced laminin adsorption on nanowires compared to flat surfaces, Colloids Surf B Biointerfaces. 122 (2014) 85–89. doi:10.1016/j.colsurfb.2014.06.048.
[40] N. Giamblanco, E. Martines, G. Marletta, Laminin adsorption on nanostructures: switching the molecular orientation by local curvature changes, Langmuir. 29 (2013) 8335–8342. doi:10.1021/la304644z.
[41] H.J. Busscher, A.W.J. van Pelt, P. de Boer, H.P. de Jong, J. Arends, The effect of surface roughening of polymers on measured contact angles of liquids, Colloid Surf. 9 (1983) 319–331. doi:10.1016/0166-6622(84)80175-4.
[42] J. Chen, C. Yan, M. Zhu, Q. Yao, C. Shao, W. Lu, J. Wang, X. Mo, P. Gu, Y. Fu, X. Fan, Electrospun nanofibrous SF/P(LLA-CL) membrane: a potential substratum for endothelial keratoplasty, Int J Nanomedicine. 10 (2015) 3337–3350. doi:10.2147/IJN.S77706.
[43] W.H. Chan, A.A. Hussain, J. Marshall, Youngs Modulus of Bruchs Membrane: Implications for AMD, Invest. Ophthalmol. Vis. Sci. 48 (2007) 2187–2187.
[44] S. Aisenbrey, M. Zhang, D. Bacher, J. Yee, W.J. Brunken, D.D. Hunter, Retinal pigment epithelial cells synthesize laminins, including laminin 5, and adhere to them through alpha3- and alpha6-containing integrins, Invest. Ophthalmol. Vis. Sci. 47 (2006) 5537–5544. doi:10.1167/iovs.05-1590.
[45] A.P. Reyes, S. Petrus-Reurer, L. Antonsson, S. Stenfelt, H. Bartuma, S. Panula, T. Mader, I. Douagi, H. André, O. Hovatta, F. Lanner, A. Kvanta, Xeno-Free and Defined Human Embryonic Stem Cell-Derived Retinal Pigment Epithelial Cells Functionally Integrate in a Large-Eyed Preclinical Model, Stem Cell Reports. 6 (2016) 9–17. doi:10.1016/j.stemcr.2015.11.008.
[46] A. Sorkio, H. Hongisto, K. Kaarniranta, H. Uusitalo, K. Juuti-Uusitalo, H. Skottman, Structure and barrier properties of human embryonic stem cell-derived retinal pigment epithelial cells are affected by extracellular matrix protein coating, Tissue Eng Part A. 20 (2014) 622–634. doi:10.1089/ten.TEA.2013.0049.
[47] A. Vallée, M.G. Faga, F. Mussano, F. Catalano, E. Tolosano, S. Carossa, F. Altruda, G. Martra, Alumina-zirconia composites functionalized with laminin-1 and laminin-5 for dentistry: effect of protein adsorption on cellular response, Colloids Surf B Biointerfaces. 114 (2014) 284–293. doi:10.1016/j.colsurfb.2013.09.053.
[48] K. Cai, H. Dong, C. Chen, L. Yang, K.D. Jandt, L. Deng, Inkjet printing of laminin gradient to investigate endothelial cellular alignment, Colloids Surf B Biointerfaces. 72 (2009) 230–235. doi:10.1016/j.colsurfb.2009.04.008.
[49] S. Peng, V.S. Rao, R.A. Adelman, L.J. Rizzolo, Claudin-19 and the barrier properties of the human retinal pigment epithelium, Invest. Ophthalmol. Vis. Sci. 52 (2011) 1392–1403. doi:10.1167/iovs.10-5984.
[50] L.J. Rizzolo, Barrier properties of cultured retinal pigment epithelium, Exp. Eye Res. 126 (2014) 16–26. doi:10.1016/j.exer.2013.12.018.
[51] J.F. Berson, D.C. Harper, D. Tenza, G. Raposo, M.S. Marks, Pmel17 initiates premelanosome morphogenesis within multivesicular bodies, Mol. Biol. Cell. 12 (2001) 3451–3464.
[52] G. Raposo, D. Tenza, D.M. Murphy, J.F. Berson, M.S. Marks, Distinct protein sorting and localization to premelanosomes, melanosomes, and lysosomes in pigmented melanocytic cells, J. Cell Biol. 152 (2001) 809–824.
[53] J.-L. Liao, J. Yu, K. Huang, J. Hu, T. Diemer, Z. Ma, T. Dvash, X.-J. Yang, G.H. Travis, D.S. Williams, D. Bok, G. Fan, Molecular signature of primary retinal pigment epithelium and stem-cell-derived RPE cells, Hum. Mol. Genet. 19 (2010) 4229–4238. doi:10.1093/hmg/ddq341.

[54] A. Georgiadis, M. Tschernutter, J.W.B. Bainbridge, K.S. Balaggan, F. Mowat, E.L. West, P.M.G. Munro, A.J. Thrasher, K. Matter, M.S. Balda, R.R. Ali, The tight junction associated signalling proteins ZO-1 and ZONAB regulate retinal pigment epithelium homeostasis in mice, PLoS ONE. 5 (2010) e15730. doi:10.1371/journal.pone.0015730.

[55] N. Esumi, S. Kachi, L. Hackler, T. Masuda, Z. Yang, P.A. Campochiaro, D.J. Zack, BEST1 expression in the retinal pigment epithelium is modulated by OTX family members, Hum. Mol. Genet. 18 (2009) 128–141. doi:10.1093/hmg/ddn323.

[56] H. Akrami, Z.-S. Soheili, M. Sadeghizadeh, K. Khalooghi, H. Ahmadieh, M.R. Kanavi, S. Samiei, J. Pakravesh, Evaluation of RPE65, CRALBP, VEGF, CD68, and tyrosinase gene expression in human retinal pigment epithelial cells cultured on amniotic membrane, Biochem. Genet. 49 (2011) 313–322. doi:10.1007/s10528-010-9409-1.

[57] P. Kay, Y.C. Yang, L. Paraoan, Directional protein secretion by the retinal pigment epithelium: roles in retinal health and the development of age-related macular degeneration, J. Cell. Mol. Med. 17 (2013) 833–843. doi:10.1111/jcmm.12070.

[58] S.C. Finnemann, E.F. Nandrot, MerTK activation during RPE phagocytosis in vivo requires αVβ5 integrin, Adv. Exp. Med. Biol. 572 (2006) 499–503. doi:10.1007/0-387-32442-9_69.

[59] C. Sheridan, P. Hiscott, I. Grierson, Retinal Pigment Epithelium Differentiation and Dedifferentiation, in: Essentials in Ophthalmology, Springer-Verlag, Berlin/Heidelberg, 2005: pp. 101–119. doi:10.1007/3-540-27152-X_7.

[60] T. Scholzen, J. Gerdes, The Ki-67 protein: From the known and the unknown, J Cell Physiol. 182 (2000) 311–322. doi:10.1002/(SICI)1097-4652(200003)182:3<311::AID-JCP1>3.0.CO;2-9.

[61] N.J. Philp, H. Yoon, E.F. Grollman, Monocarboxylate transporter MCT1 is located in the apical membrane and MCT3 in the basal membrane of rat RPE, Am. J. Physiol. 274 (1998) R1824–8.

[62] B.M. Kevany, K. Palczewski, Phagocytosis of retinal rod and cone photoreceptors, Physiology (Bethesda). 25 (2010) 8–15. doi:10.1152/physiol.00038.2009.

[63] K.S. Boochoon, J.C. Manarang, J.T. Davis, A.M. McDermott, W.J. Foster, The influence of substrate elastic modulus on retinal pigment epithelial cell phagocytosis, J Biomech. 47 (2014) 3237–3240. doi:10.1016/j.jbiomech.2014.06.021.

[64] C.A. Curcio, K.R. Sloan, R.E. Kalina, A.E. Hendrickson, Human photoreceptor topography, J Comp Neurol. 292 (1990) 497–523. doi:10.1002/cne.902920402.

[65] M.G. Pilgrim, I. Lengyel, A. Lanzirotti, M. Newville, S. Fearn, E. Emri, J.C. Knowles, J.D. Messinger, R.W. Read, C. Guidry, C.A. Curcio, Subretinal Pigment Epithelial Deposition of Drusen Components Including Hydroxyapatite in a Primary Cell Culture Model, Invest. Ophthalmol. Vis. Sci. 58 (2017) 708–719. doi:10.1167/iovs.16-21060.

[66] B.B. Thomas, D. Zhu, L. Zhang, P.B. Thomas, Y. Hu, H. Nazari, F. Stefanini, P. Falabella, D.O. Clegg, D.R. Hinton, M.S. Humayun, Survival and Functionality of hESC-Derived Retinal Pigment Epithelium Cells Cultured as a Monolayer on Polymer Substrates Transplanted in RCS Rats, Invest. Ophthalmol. Vis. Sci. 57 (2016) 2877–2887. doi:10.1167/iovs.16-19238.

[67] M.R. Antognazza, M. Di Paolo, D. Ghezzi, M. Mete, S. Di Marco, J.F. Maya-Vetencourt, R. Maccarone, A. Desii, F. Di Fonzo, M. Bramini, A. Russo, L. Laudato, I. Donelli, M. Cilli, G. Freddi, G. Pertile, G. Lanzani, S. Bisti, F. Benfenati, Characterization of a Polymer-Based, Fully Organic Prosthesis for Implantation into the Subretinal Space of the Rat, Adv Healthc Mater. (2016). doi:10.1002/adhm.201600318.

[68] L. Vroman, A.L. Adams, M. Klings, G. Fischer, Fibrinogen, Globulins, Albumin and Plasma at Interfaces, in: Advances in Chemistry, AMERICAN CHEMICAL SOCIETY, WASHINGTON, D. C, 1975: pp. 255–289. doi:10.1021/ba-1975-0145.ch012.

[69] B.V. Stanzel, Z. Liu, S. Somboonthanakij, W. Wongsawad, R. Brinken, N. Eter, B. Corneo, F.G. Holz, S. Temple, J.H. Stern, T.A. Blenkinsop, Human RPE stem cells grown into polarized RPE monolayers on a polyester matrix are maintained after grafting into rabbit subretinal space, Stem Cell Reports. 2 (2014) 64–77. doi:10.1016/j.stemcr.2013.11.005.

[70] M.J. Koss, P. Falabella, F.R. Stefanini, M. Pfister, B.B. Thomas, A.H. Kashani, R. Brant, D. Zhu, D.O. Clegg, D.R. Hinton, M.S. Humayun, Subretinal implantation of a monolayer of human embryonic stem cell-derived retinal pigment epithelium: a feasibility and safety study in Yucatán minipigs, Graefes Arch. Clin. Exp. Ophthalmol. 254 (2016) 1553–1565. doi:10.1007/s00417-016-3386-y.

Table 1: Electrospinning Parameters for Fabrication of Nanofibrous Membranes

Electrospinning Parameters	Polymers			
	PCL	PLGA	PLDLA	PLLA
Polymer Concentration (w/v%)	4	1	0.5	0.5
Solvents HFIP:PBS (v/v%)	9:1	9:1	9:1	9:1
Flow rates (mL/hr)	1	1	1	1
Voltage (kV)	15	15	15	15
Working Distance (cm)	15	15	15	15

Table 2: List of Oligo Sequences for each of the Genes and GAPDH

Gene	Sense	Antisense
GAPDH	AGA AGG CTG GGG CTC ATT TG	AGG GGC CAT CCA CAG TCT TC
PMEL17	GTT GAT GGC TGT GGT CCT TG	CAG TGA CTG CTG CTA TGT GG
ZO1	CAA CAT ACA GTG ACG CTT CAC A	CAC TAT TGA CGT TTC CCC ACT C
BEST1	CAT GAG CTG GAC CTC GTT GT	CCA ACA GGG ACA CCT GCA AA
RPE65	CAA GGC TGA CAC AGG CAA GA	TTG ACG AGG CCC TGA AAA GA
PEDF	TTC AAA GTC CCC GTG AAC AAG	GAG AGC CCG GTG AAT GAT GG
VEGF	GCA GAA TCA TCA CGA AGT GGT	TAT GTG CTG GCC TTG GTG AG
MerTK	GCC CGG ACA GGG AGC TT	TGC CTC AGT GAT AGC TCT ACG
LAMP2	TGG CAA TGA TAC TTG TCT GCT G	ACG GAG CCA TTA ACC AAA TAC AT

Table 3: Physical and Chemical Properties of Polymers

Polymers	Monomer Composition	M_n (kDa)	PDI	T_g (°C)	T_m (°C)	X_c (%)
PCL	100	121	1.5	- 61	62	50
PLGA	85:15	134	1.4	54	130	26
PLDLA	70:30	148	1.3	58	144	30
PLLA	100	142	1.2	66	180	38

Table 4: Surface and Physical Properties of Electrospun Nanofibrous Membranes (ENMs)

Polymers	Fibre Diameter (nm)	Membrane Thickness (µm)	Porosity (%)	Contact Angle (°)	Surface Roughness (RMS) (nm)	Surface Stiffness (N/m)	Modulus (MPa)
PCL	64 ± 2	1.01 ± 0.03	50 ± 2	89 ± 4 *	261 ± 4	0.48 ± 0.02	16 ± 1 **
PLGA	70 ± 8	1.03 ± 0.03	49 ± 2	105 ± 3 **	258 ± 9	0.51 ± 0.04	25 ± 4
PLDLA	67 ± 2	1.04 ± 0.03	49 ± 2	110 ± 2	264 ± 5	0.72 ± 0.06 *	31 ± 6 **
PLLA	65 ± 2	1.06 ± 0.03	51 ± 2	118 ± 2 **	269 ± 6	0.84 ± 0.05 *	48 ± 5 *

n = 100 for fibre diameters, n = 50 for membrane thickness, n = 50 for porosity, n = 10 for contact angle, and n = 6 for surface roughness, surface stiffness and modulus, where n is number of samples per group.
Data presented as mean ± SE
** denotes statistically difference between groups ($p < 0.05$)
* denotes a significant difference from other groups ($p < 0.05$).

Figure Captions

Figure 1: SEM images depicting electrospun fibre diameter (Fig. 1A-1D), and membrane thicknesses for the ENMs (the yellow arrows indicated the top and bottom surfaces of the ENMs, Fig. 1A"-1D"), and fibre diameter distribution (Fig. 1A'-1D'). Fig. 1A-1D scale bar 20 μm, and Fig. 1A"-1D" scale bar 2 μm.

Figure 2: 2D and 3D Atomic force microscopy (AFM) images of the ENMs. Area analyzed 10 μm x 10 μm.

Figure 3: Adsorption of laminin on the surface of the ENMs and controls. Data expressed as the mean ± SE, and n = 6 per group. ** denotes significant difference between groups ($p < 0.05$). * denotes significant difference from all other groups ($p < 0.05$). Scale bar 50 μm for all images.

Figure 4: SEM images of hRPE cells cultured on the ENMs and controls. Fig. 4A-4E, 4A'-4E' and 4A"-4E" represent Week 1. Fig. 4F-4J, 4F'-4J' and 4F"-4J" represent Week 2. Fig. 4K-4O, 4K'-4O' and 4K"-4O" represents Week 4, and Fig. 4P-4T, 4P'-4T' and 4P"-4T" represents Week 8. Fig. 4A-4T scale bar 200 μm, Fig. 4A'-4T' scale bar 10 μm, and Fig. 4A"-4T" scale bar 5 μm.

Figure 5: WST-1 assay for hRPE cells cultured on ENMs and controls. Data expressed as the mean ± SE, and n = 6 per group, per time point. *** denotes significant difference between each of the time points ($p < 0.05$). ** denotes significant difference between groups at each time point ($p < 0.05$). * denotes significant difference from all other groups at each time point ($p < 0.05$).

Figure 6: TER measurements of hRPE cells cultured on the ENMs. Data expressed as the mean ± SE, and n = 6 per group, per time point. *** denotes significant difference from all other time points ($p < 0.05$). ** denotes significant difference between groups at each time point ($p < 0.05$). * denotes significant difference from all other groups at each time point ($p < 0.05$).

Figure 7: Gene expression of hRPE cells cultured on the ENMs normalized to week 2 controls. Data expressed as the mean ± SE, and n = 4 per group, per time point. *** denotes significant difference between time points ($p < 0.05$). * denotes significant difference from all other groups at each time point ($p < 0.05$).

Figure 8: Immunohistochemical assessment of hRPE cells cultured on the ENMs and controls. Fig. 8A-8O represent Week 2. Fig. 8A'-8O' represent Week 4. Fig. 8A"-8Y" represents Week 8. Fig. 8A-8E, Fig. 8A'-8E' and 8A"-8E" represent Cytokeratin18 (Ck18) and Ki67. Fig. 8F-8J, Fig. 8F'-8J' and 8F"-8J" represent ZO1. Fig. 8K-8O, Fig. 8K'-8O' and 8K"-8O" represent MITF. Fig. 8P"-8T" represent MCT1, and Fig. 8U"-Y" represent MerTK. Scale bar 50 μm for all images.

Figure 9: Phagocytosis of hRPE cells cultured on the ENMs and controls at Week 8. Fig. 9A-9E represent trypsinized single hRPE cells obtained from intact hRPE monolayers (blue arrows: non phagocytosed beads, and black arrows: phagocytosed beads). Fig. 9F represents number of beads phagocytosed per hRPE cell, and percentage phagocytosing cells. Data expressed as the mean ± SE, and n = 100 per group. * denotes significant difference from all other groups ($p < 0.05$). Scale bar 50 μm for all images.

Figure 10: TEM images of hRPE cells cultured on the PLLA ENMs. Fig. 9A-9A" represent Week 4. Fig. 9B-9B" represent Week 8. Fig. 9A and 9B scale bar 5 μm. Fig. 9A', 9A", 9B' and 9B" scale bar 2 μm.

Figure 11: *In vivo* assessment of implanted 70 nm PLLA ENMs. Fig. 11A and 11A' represent fundus and OCT at Week 1. Fig. 11B-11D represent H&E, and Fig. 11B'-11D' represent immunofluorescent staining for sham controls and rat eyes implanted with PLLA ENMs at Weeks 1 and 4. * in figures depict position of implanted PLLA ENMs. Fig. 11E represents quantitative analysis of microglial cells (Iba1) for sham operated controls and rat eyes implanted with PLLA ENMs at Weeks 1 and 4. Fig. 11F represents thickness and # of rows of cells in the ONL for sham operated controls and rat eyes implanted with PLLA ENMs at Weeks 1 and 4. Fig. 11B-11D scale bar 50 μm. Fig. 11B'-11D' scale bar 200 μm. * in Fig. 11E and 11F denotes significant difference from all other groups ($p < 0.05$). ENM: electrospun nanofibrous membrane, ONL: outer nuclear layer, INL: inner nuclear layer, IPL: inner plexiform layer and GCL: ganglion cell layer.

Age related macular degeneration (AMD) is a leading cause of vision loss in the developed world, with an increasing number of people suffering from blindness or severe visual impairment. Transplantation of retinal pigment epithelium (RPE) cells supported on a synthetic, biomimetic-like Bruch's membrane (BM) is considered a promising treatment. However, the synthetic scaffolds used do not mimic the microenvironment of the RPE cell supporting layers, required for the development of a functional RPE monolayer. This study indicated that porous, laminin coated, 70 nm PLLA ENMs supported functional RPE monolayers, exhibiting 3D polygonal-cobblestone morphology, apical microvilli, basal infoldings, high transepithelial resistance (TER), phagocytic activity and expression of signature RPE markers. These findings indicate the potential clinical use of porous, laminin coated, 70 nm PLLA ENMs in fabricating retinal constructs aimed at treating dry AMD.